International Journal of
Science and Engineering Investigations vol. 8, issue 91, August 2019
Received on August 22, 2019 ISSN: 2251-8843

A Complete Identification Methodology for Identifying Parameters of Twin Rotor Multi Input Multi Output System (TRMS)

Muhammad Aziz Omar Kandel[1], M. Elsamanty[2], S. AbdRaboo[3], Yehia H. Hossamel-din[4]
[1,2,3]Department of Mechanical Engineering, Shobra Faculty of Engineering, Benha University
[2]Department of Mechanical Engineering, School of Engineering and Applied Sciences, Nile University
[4]Head of Mechanical Engineering Dept - Future University in Egypt (FUE)
([1]azizforever20010@yahoo.com, [2]Mahmoud.alsamanty@feng.bu.edu.eg, [3]saberabdrabbo@yahoo.com, [4]Yehia.hendawy@fue.edu.eg)

Abstract-In this paper a complete study for modelling the TRMS and estimating all its parameters using grey box system identification technique. The identification process starts with identifying the TRMS inputs/outputs terminals pinout. A MyRIO kit is used for all measurements and controlling the whole TRMS. A complete precise and accurate SOLIDWORKS model for the whole TRMS is built to estimate any missing parameters. The next step in the identification process is dissembling the TRMS into basic components whose input/output relation need to be identified. Dynamic equations are used to aggregate the identified components with the remaining TRMS parts. Finally, an accurate and precise two degree of freedom (2-DOF) model for the TRMS are obtained.

Keywords- *Twin Rotor Multi Input Multi Output System(TRMS), System Identification, Helicopter, Paramter Estimation.*

I. INTRODUCTION

Helicopter one of powerful systems invented by human. In 1923 Cierva autogiro built the first rotary-wing aircraft and his invitation was able to fly successfully [1]. Now days helicopters enter many disciplines and its importance to human life gradually increased. Helicopter is complicated systems which perform tasks can't be achieved by the classical airplane. Helicopter has the advantage of vertical take-off and landing and hovering left and right easily, which make it a perfect solution to fly inside narrow environments [2]. Recently, Helicopter applications increased rapidly specially unmanned helicopters and humans tends to perform dangerous and complicated tasks using helicopters such as firefighting [3] and mine detection and sweeping, flying ambulances [4] also helicopters can be used for in heavy and fast transportation of supplies and humans [5] also helicopters can be used for traffic monitoring and television photography [6]. However, helicopters have two major problems, first one is the strong coupling relationship that exist between the helicopter inputs and outputs [2] where each motor rotate generate thrust force in one direction and coupling moment in the other direction, second one is the high nonlinearity that exist between the helicopter inputs .

To study the dynamics of the helicopters and test different control theories a simpler laboratory model for the helicopter is used, this model is called Twin Rotor Multi Input Multi Output System TRMS [7]. Real helicopters are difficult to study and collect data from it in labs, here the importance of the TRMS model appear which reassembly and simulate and retain the main characteristics of the real helicopters and can be tested and collect data from it easily in labs. The TRMS is shown in figure 1, TRMS consists of a beam pivoted on its base in such a way that it can rotate freely both in the horizontal and vertical planes. At both ends of the beam there are rotors (the main and tail rotors) driven by DC motors. Each motor has a built in tacho generator to measure the motor rotating speed. A counterbalance arm with a weight at its end is fixed to the beam at the pivot. Two incremental encoders fixed at the axis of rotation of each angle to measure the yaw and pitch angles.

Figure 1. TRMS

Several studies work on modeling the TRMS using different techniques. A 1DOF black box system identification model has been introduced [8] and developed based on experimental data. To obtain this model, the TRMS is

subjected to different level step input signals while recording the pitch output response. Then the outputs and inputs data are correlated using ARMX identification method using MATLAB system identification toolbox.

A neural network model has been introduced [9] and developed based on the experimental data. The presented model was used to obtain a mathematical model that correlates the model parameters with the system output. Moreover, another method [10] is derived based on the parametric linear approach to obtain the TRMS model. However, it can be noticed that the twisting torque of the cable has been ignored which in real affect the overall performance of the controller. Furthermore, it has been assumed that the model is working under single degree of freedom model.

In this paper a grey box system identification technique is chosen to identify the TRMS. All the TRMS parts are identified based on input-output relationship of the different TRMS parts with the aid of physical relationship. The cables twisting torque issue is solved by replacing the cables with very flexibles cable and fixing them in a way that almost vanish the remaining cables twist torque. as shown in figure 2 and figure 3.

Figure 2. Pitch angle cable

Figure 3. Yaw angle cable

The procedure for identifying the TRMS start in section II with writing the mathematical equations that describe the whole system using newtons law of motion. In section III a several experimental tests for the TRMS components to estimate input/output relation and any missing parameters like speed/ thrust force propellers relationship, tacho generators speed/output voltage, system mass moment of inertial in pitch and yaw direction. In section IV all the relationship and parameters from section III and equations from section II are aggregated to generate 1 DOF pitch model and 1 DOF yaw model and 2 DOF whole system model. In section V the results are presented and the real system response and model response are compared.

II. TWIN ROTOR DYNAMICS

The TRMS is 2 DOF coupled system, for studying its dynamics the equation of motion in pitch direction is written first (Equation 1 and 2), including all the forces and torques that govern the motion is this direction. The free boy diagram of the TRMS in pitch direction shown in figure 4, by writing the equation of motion in pitch direction the following moments governs the TRMS motion in pitch direction: the moment due to main rotor thrust force (M_m) which equals the main motor thrust force (F_M) times the distance $l_m$which starts from the center of main rotor (A) to center of rotation O , the tail coupling moment (M_{CT}) which is a reaction moment arise from the from the rotation of the tail propeller , this moments equals to the tail coupling force (F_{CTM}) times l_m , the moment due to the gravity force of the connecting rod (M_r) which equal to the of the TRMS connected rod mass m_p including the mass of the motors and propellers times the cosine component of the pitch angle θ_P times the distance l_p which starts from the center of mass of the connecting rod to the center of rotation O times the gravitational acceleration g $(9.81\ \mathrm{m/s^2})$, the moment due to the gravity force of the counter balance weight (M_{CB}) which equal to the of the counter balance weight mass m_c times the cosine component of the pitch angle θ_P times the distance l_c which starts from the center of mass of the counter balance weight to the center of rotation O times the gravitational acceleration g , and finally the friction torque in pitch direction (T_{fP}).

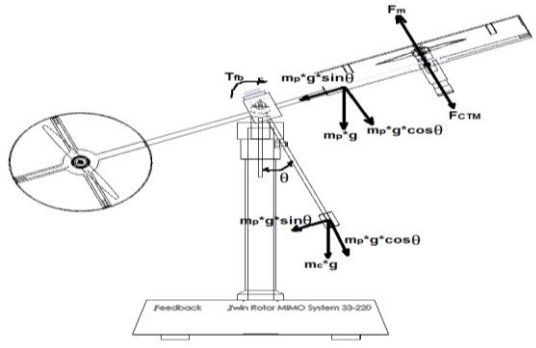

Figure 4. TRMS free body diagram in pitch direction

$$\curvearrowleft + \sum_O M = J_p.\frac{d^2\theta_P}{d^2t} \quad (1)$$

$$F_M.l_m - m_p.g.l_p.\sin(\theta_P) - m_c.g.l_c.\cos(\theta_P) - T_{fp} - F_{CTM}.l_m = J_P * \frac{d^2\theta_P}{d^2t} \quad (2)$$

where J_P ….. mass moment of inertia in pitch direction

The free boy diagram of the TRMS in yaw direction shown in figure 5 TRMS free body diagram in yaw direction, by writing the equation of motion in yaw direction (Equation 3 and 4), the following moments governs the TRMS yaw angle θ_T: the moment due to tail rotor thrust force (Mt) which equals the tail motor thrust force (F_t) times the distance l_t which starts from the center of tail rotor (B) to center of rotation O , the main coupling moment (M_{CM}) which is a reaction moment arise from the from the rotation of the main propeller , this moments equals to the main coupling force (F_{CMT}) times l_t , and finally the friction torque in pitch direction (T_{fy}).

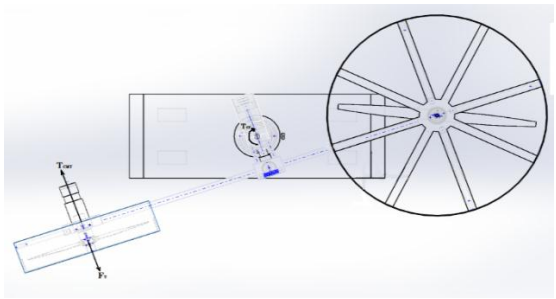

Figure 5. TRMS free body diagram in yaw direction

$$\curvearrowleft + \sum_O M = J_T * \frac{d^2\theta_T}{d^2t} \quad (3)$$

$$F_T * l_t - F_{CMT} * l_t - T_{fy} = J_T * \frac{d^2\theta_T}{d^2t} \quad (4)$$

III. PARAMETERS ESTIMATION AND SUBSYSTEMS IDENTIFICATION

In this section all the system parameters are estimated. Any subsystems which can't be described by the mathematical equation is identified experimentally. By recording the input/output relationship for any subsystem, the mathematical model is deduced. This section is divided into three parts, the first part deal with explicit parameters estimation. The Second part deal implicit parameters estimations. The Third part deal with identified parameters and subsystems.

A. Explicit parameters estimation

In this part all the parameters which can be measured directly is obtained. To achieve this goal and allow any future measurements, the TRMS is disassembled and all its parts are measured and weighted using calibrated electronic scale. Then a complete accurate and precise SOLIDWORKS model for the whole TRMS is drawn. From the SOLIDWORKS model, the following parameters are specified in table 1.

TABLE I. SOLIDWORKS EXPLICIT TRMS PARAMETERS

Parameter	Value	Unit
l_m	0.25	m
l_p	0.010745	m
l_c	0.22557097	m
l_t	0.2275	m
m_p	0.99072840335	kg
m_c	0.08872180	kg
J_P	0.06352981	kg. m^2

B. Implicit parameters estimation

In this part parameter which need some calculations and can't be measured directly is estimated.

The value of the mass moment of inertia J_y is not fixed like J_P it depends upon the pitch angle $\boldsymbol{\theta}_p$. analyzing the system show that

$$J_y = m_p.{l_p}^2.\cos^2(\boldsymbol{\theta_p}) + m_c.{l_c}^2.\sin^2(\boldsymbol{\theta_p}) + m_c.d^2 + J_r \quad (5)$$

The term $m_r.{l_r}^2.\cos^2(\boldsymbol{\theta_p})$ is the moments of inertia of the connecting rod with the propeller. The term $m_c.{l_r}^2.\sin^2(\boldsymbol{\theta_p})$ *is* moments of inertia of the counter balance weight. Due to eccentricity, the term $m_c.d^2$ is added as a result of the parallel axis theorem, where d is the distance between two centers. Finally, a fixed inertia J_r is added due to rotation of the vertical rod carrying the connecting rod. Using SOLIDWORKS model the required parameter values is specified in Table 2.

TABLE II. SOLIDWORKS PARAMETERS FOR J_y ESTIMATION

Parameter	Value	Unit
d	0. 0.05210000	m
J_r	0.0002538581725	kg. m2

C. Identified parameters and subsystems

In this part parameters and subsystems which can't be estimated implicitly or explicitly are identified. The inputs and outputs are recorded and then exported to MATLAB environment to deduce the proper subsystem model. Investigating the equation of motion of pitch and yaw direction, the following terms need to be identified F_M , F_{CTM} , T_{fp} , F_T , F_{CMT} , T_{fy} . Staring with the thrust forces F_M & F_T these forces is controlled only the motor angular velocities (ω_m & ω_t) of the main and tail propellers (fixed bald angles propellers), the relation between the velocities and the thrust forces are directly proportional. The value of (ω_m & ω_t) are determined by the dc motors supplied voltages U_m & U_t. Before identifying the relationship between U_m vs ω_m and U_t vs ω_t the built in tacho generators constants in dc motors will be first identified.

- Tacho generator

The tail and main motors are the same MAXON M97845, they assumed to have the same characteristics, so this test is achieved for one motor only. To identify the tacho generator constant, the propeller is removed to allow the dc motors rotate freely and reach the maximum speed in both directions, then the dc motors are supplied by stairs input signal from a MYRIO controller kit, with increment voltage 0.1 and delay time 2 second between each increment to allow the tacho output voltage to be settled. The dc motor rotation speed is measured using external incremental encoder fixed to the axis of the motor shafts and an optocouplers sensor is fixed to the motor bases to detect the motor movement as shown in figure 6. the optocoupler output pulses is sensed and measure using MYRIO interrupt input to estimate the motors rotational speed. The supplied voltages from the MYRIO and the estimated encoder speed are recorded through a LabVIEW vi built to monitor and record all these data. A graph for the results is presented is section V.

Figure 6. External incremental encoder & Optocoupler

After analyzing the pervious data tacho generator constant K_M & K_t are estimated as ≈174.41 (rad/sec)/V

- Propeller speed ($\omega_{m\,\&}\,\omega_t$)

After fixing the propeller again to the motor they are treated as a single element whose input/output relation need to be identified. The motor voltage level is the input and the propeller speed are the output. The motor is supplied with step input signals with different levels using MYRIO kit. The propeller speed is the measured from the tacho generator. A LABVIEW GUI is built to generate the input signal and measure & record the output signal. The input signal and output signal are exported to the MATLAB system identification toolbox to deduce the input/output transfer function. The tail and main propellers are not the same size, so these procedures are applied once for the tail and once for the main. A graph for the output data is presented in section 7. The following transfer functions are obtained.

Main transfer function: $\frac{117}{S+1.37}$ (6)

Tail transfer function: $\frac{705}{S+3.72}$ (7)

The obtained model from the tail and the main is validated using square input signal.

- Propeller thrust force (F_M , F_T)

To deduce the relation between the propellers thrust force and the propellers speed a special test rig show in figure 7 is used. The test rig consists from a 1kg load cell to measure the thrust force. A 24-bit analog to digital converter HX711 to measure the load cell output voltage and send it to MYRIO kit through serial port. A LabVIEW GUI to collect the ADC data and estimated the thrust force and change the propeller motor input voltage. The motor voltage is allowed from 0V (minimum voltage) to +5v (maximum voltage). The voltage is incremented 0.1v every 5 second to allow the propeller thrust force to be settled.

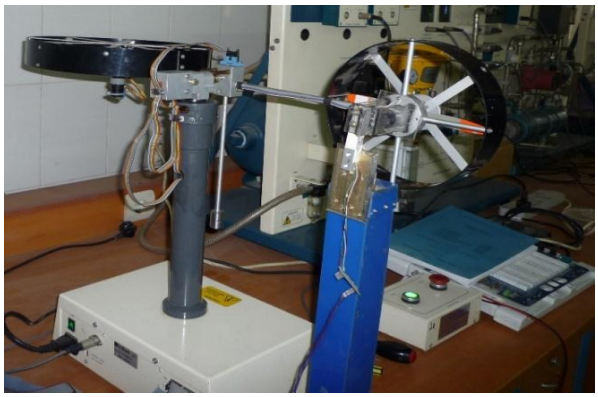

Figure 7. Thrust measuring test rig

Main Thrust force speed relation

$M(x)=3.31297472111087e^{-06}.x^3 + 0.0004131403925287.x^2 + 0.119043893271919.x - 0.179162803963625$ (8)

Where

M(x) …… Main Propeller Thrust Force [gm]

x …… Main Propeller Rotation Speed [rad/sec]

Tail Thrust force speed relation

$T(y) = 2.59000552842777e^{-07}. y^3 - 4.56181484583037e^{-05}. y^2 + 0.0190605599207999.y$ (9)

Where

T(y) …… Tail Propeller Thrust Force [gm]

y …… Tail Propeller Rotation Speed [rad/sec]

- Propeller coupling force (F_{CTM} , F_{CMT})

To estimate the coupling force that each rotor exerts in the other rotor direction, the same test rig for measuring the thrust is used. Each rotor speed is incremented gradually while measuring thrust force exert in the other rotor direction as shown in figure 8 and figure 9.

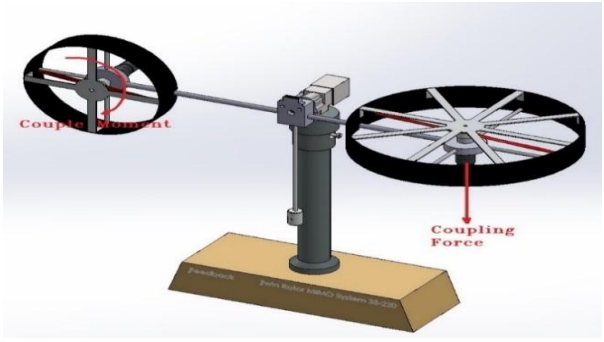

Figure 8. Coupling force due to main rotor rotation

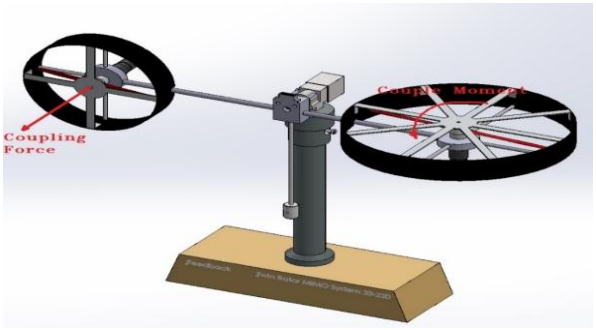

Figure 9. Coupling force due to tail rotor rotation

Coupling force on Main due to tail rotation:

$P(x) = 1.45744214558762e^{-07}.\ y^3 - 1.36357137032624e^{-05}.\ y^2 - 0.00244527531967665.y - 0.0692160673963882$ (12)

Where:

P(y) …… Coupling Force on Main Propeller [gm]

y …… Tail Propeller Rotation Speed [rad/sec]

Coupling force on tail due to main rotation:

$Q(x) = 4.92948629293795e^{-07}.x^3 + 4.20472796444510e^{-05}.x^2 + 0.0150443581122425.x + 1.02728277048537$ (13)

Where

Q(x) …… Coupling Force on Tail Propeller [gm]

x …… Main Propeller Rotation Speed [rad/sec]

- Friction Torque (T_{fp} ,T_{fy})

The friction torque depends on the angular velocity of the rotors connecting rod (Ω) and the damping coefficient (B_p) in that direction.

$$T_{fp} = B_p.\Omega_p \quad (14)$$

$$T_{fy} = B_y.\Omega_y \quad (15)$$

Using unforced damping oscillation, the damping coefficient in pitch and yaw direction (B_p , B_y) can be estimated. To estimate B_p the connected rod is moved from rest 10° then it's allowed to oscillate freely. Recording the system output response, the damping coefficient is estimated. The equation of motion that described the system in free oscillation is for small angles

$\sin(\theta)$ equals θ , where θ *in radian* for Viscous friction

$$T_f = -B * \frac{d\theta}{dt} \quad (16)$$

$$J * \frac{d^2\theta}{d^2t} + B * \frac{d\theta}{dt} + m * g * l * \theta + m * g * l_r * \theta = 0 \quad (17)$$

$$\frac{d^2\theta}{d^2t} + \frac{B}{J} * \frac{d\theta}{dt} + \frac{m*g*l+m*g*l_r}{J} * \theta = 0 \quad (18)$$

this equation can be written in the standard form as

$$\frac{d^2\theta}{d^2t} + 2 * \zeta * w_n * \frac{d\theta}{dt} + {w_n}^2 * \theta = 0 \quad (19)$$

where:

$$2 * \zeta * w_n = \frac{B}{J} \quad (20)$$

$${w_n}^2 = \frac{m*g*l+m*g*l_r}{J} \quad (21)$$

$$w_n = w_d * \sqrt{1-\zeta^2} \quad (22)$$

To estimate the damping coefficient in yaw direction B_y the TRMS is rotated 90° to allow the connecting rod oscillate freely in yaw direction. Then the same previous procedure is applied.

IV. MODEL BUILDING AND TESTING

In this section all, estimated parameters and identified subsystems are aggregated to generate complete models. The generated models are tested in open loop mode in simulation and experimentally using step input and square signals. Although open loop responses are not enough to accept these models, but it gives elementary indication about model goodness. This section is divided into three part, 1 DOF vertical model building, 1 DOF horizonal model building, and 2 DOF model building.

A. Building and testing 1 DOF vertical model

From the previous data, all the dynamic equations that describe the TRMS behavior in 1 DOF vertical motion are presented.

$$\circlearrowleft + \sum_O M = J_p.\frac{d^2\theta_P}{d^2t} \quad (23)$$

$$0.25.F_M - 0.1044311453680983.\sin(\theta_P) - 0.1963281429890923.\cos(\theta_P) - 0.005618696.\frac{d\theta_P}{dt} = 0.06352981.\frac{d^2\theta_P}{d^2t} \quad (24)$$

$$F_M = 3.31297472111087e^{-06}.\ {\omega_m}^3 + 0.000413140392528774.\ {\omega_m}^2 + 0.119043893271919.\ \omega_m - 0.179162803963625 \quad (25)$$

$$\frac{\omega_m}{U_m} = \frac{117}{S+1.37} \quad (26)$$

B. Building and testing 1 DOF horizontal model

From the previous data, all the dynamic equations that describe the TRMS behavior in 1 DOF horizonal motion are presented

$$\text{ل} + \sum_O M_T = J_T.\frac{d^2\theta_T}{d^2t} \quad (27)$$

$$0.2275\,.F_T - 0.006855905.\frac{d\theta_T}{dt} = \left(1.143845725769843e^{-4}\cos^2(\boldsymbol{\theta_p}) + 0.0045143659176706.\sin^2(\boldsymbol{\theta_p}) + 2.40827341138.e^{-6} + 0.0002538581725839\right).\frac{d^2\theta_T}{d^2t} \quad (28)$$

$$\frac{\omega_t}{U_t} = \frac{705}{S+3.72} \quad (29)$$

C. Building and testing 2 DOF model

Combining the equations from part A and part B, and adding the coupling effect of each rotor in the other direction, a 2 DOF model is completely specified.

$$\text{ل} + \sum_O M_P = J_p * \frac{d^2\theta_P}{d^2t} \quad (30)$$

$$0.25.(F_M - F_{CTM}) - 0.1044311453680983\,.\sin(\theta_P) - 0.1963281429890923\,.\cos(\theta_P) - 0.005618696.\frac{d\theta_P}{dt} = 0.06352981.\frac{d^2\theta_P}{d^2t} \quad (31)$$

$$\text{ل} + \sum_O M_T = J_T.\frac{d^2\theta_T}{d^2t} \quad (32)$$

$$0.2275.(F_T - F_{CMT}) - 0.006855905.\frac{d\theta_T}{dt} = [1.143845725769843e^{-4}\cos^2(\boldsymbol{\theta_p}) + 0.0045143659176706\sin^2(\boldsymbol{\theta_p}) + 2.40827341138e^{-6} + 0.000253858172583].\frac{d^2\theta_T}{d^2t} \quad (33)$$

F_M=3.31297472111087e^{-06}. ω^3 + 0.000413140392528774. ω_m^2 + 0. 119043893271919.ωm - 0.179162803963625 (34)

F_{CMT} = 4.92948629293795e^{-07}. ω_m^3 + 4.20472796444510. e^{-05}.ω_m^2+0.0150443581122425.ω_m+1.02728277048537 (35)

$$\frac{\omega_m}{U_m} = \frac{117}{S+1.37} \quad (36)$$

F_T = 2.59000552842777e^{-07}. ω_t^3 - 4.56181484583037e^{-05}. ω_t^2 + 0.0190605599207999. ω_t (37)

F_{CTM} = 1.45744214558762e^{-07}. ω_t^3 -1.36357137032624e^{-05}. ωt^2 -0.00244527531967665.ω_t - 0.0692160673963882 (38)

$$\frac{\omega_t}{U_t} = \frac{705}{S+3.72} \quad (39)$$

V. RESULTS

Figure 10 displays the relation between the rotational speed of the dc motor (tail or main) and the output voltage from the tacho gereator coupled with each motor. The graph shows that, they are linearly related, with a straight line whose slope equals 174.41 (rad/sec)/V.

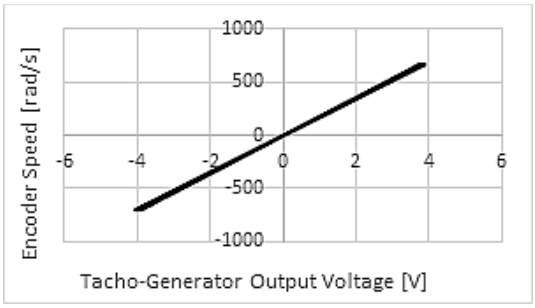

Figure 10. Tacho generator calibration data

Figure 11 displays, a comparison between the real speed step signal response of the main dc motor coupled with the main propeller and, the simulated speed step response. A step response signal is chosen to generate the simulated model for the dc motor coupled with the main propeller. From the graph it is appear that, the real response and the simulated response are mainly fitted with a fitting percent more than 95%.

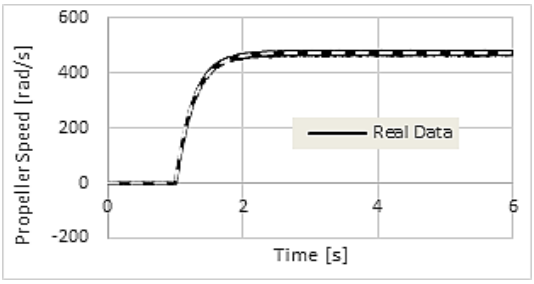

Figure 11. Real step response for main dc motor & propeller subsystem vs model

Figure 12 displays a comparison a comparison between the real square signal speed response of the main dc motor coupled with the main propeller and, the simulated speed step response. A square signal is chosen to be a validation signal to test the quality of the simulated subsystem model response obtained from the step response. From the graph it is shown, that the simulated subsystem square response is fitted with the real response with 91%, so the simulated model is valid to describe all the motor real dynamics.

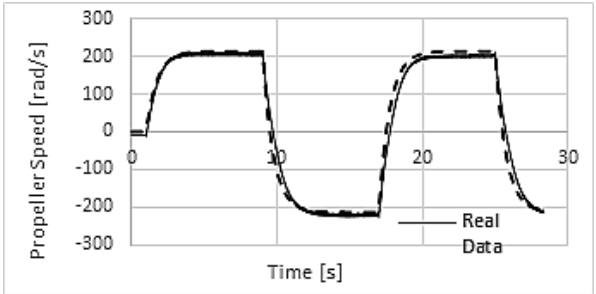

Figure 12. Main dc motor & propeller subsystem model verification using square signal

Figure 13 displays, a comparison between the real speed step signal response of the tail dc motor coupled with the tail propeller and, the simulated speed step response. A step response signal is chosen to generate the simulated model for the dc motor coupled with the tail propeller. From the graph it is appear that, the real response and the simulated response are mainly fitted with a fitting percent more than 95%.

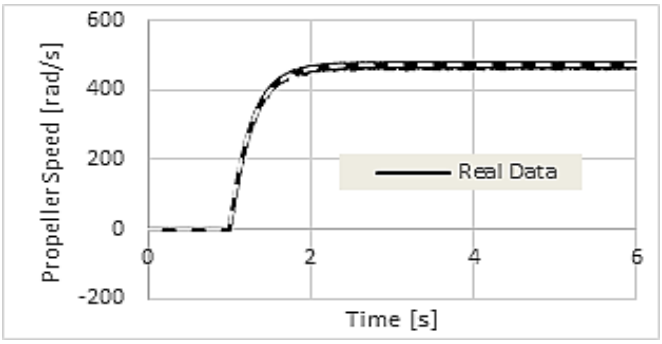

Figure 13. Real step response for tail dc motor & propeller subsystem vs model

Figure 14 displays a comparison a comparison between the real square signal speed response of the tail dc motor coupled with the tail propeller and, the simulated speed step response. A square signal is chosen to be a validation signal to test the quality of the simulated subsystem model response obtained from the step response. From the graph it is shown, that the simulated subsystem square response is fitted with the real response with 91%, so the simulated model is valid to describe all the motor real dynamics.

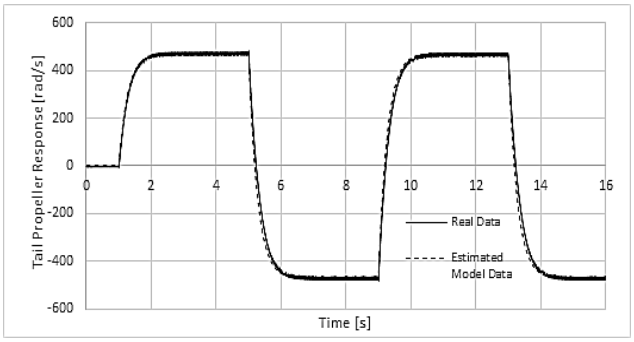

Figure 14. Tail dc motor & propeller subsystem model verification using square signal

Figure 15 explains the relation between the main propeller thrust force and propeller rotational speed. These data in this graph are the real measurements excluded from the main propeller thrust test. This graph is used to generate an estimated model for the main propeller, that describe the main propeller thrust-speed relation.

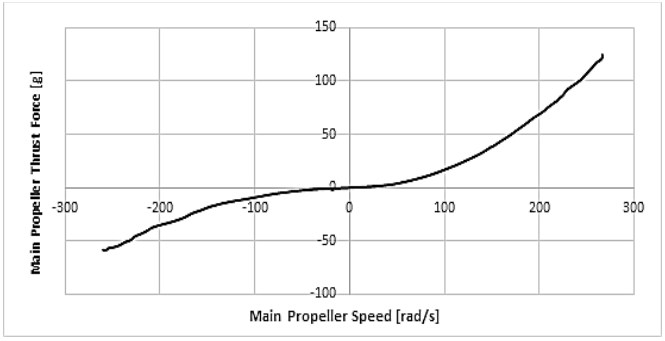

Figure 15. Main propeller real speed/Output thrust relationship

Figure 16 shows a comparison between real data obtained from the main propeller thrust test and, the generated model for the main propeller thrust-speed relation. From the graph, it's shown that the model is 90% fitted with the real data.

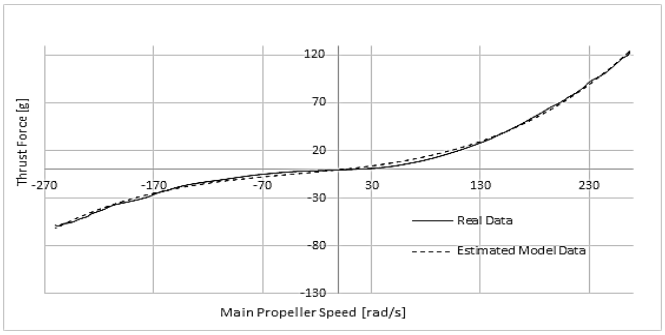

Figure 16. Real tail rotor speed/Coupling force on main relationship

Figure 17 explains the relation between the tail propeller thrust force and propeller rotational speed. Thes data in this graph are the real measurements excluded from the tail propeller thrust test. This graph is used to generate an estimated model for the tail propeller that describes the tail propeller thrust-speed relation.

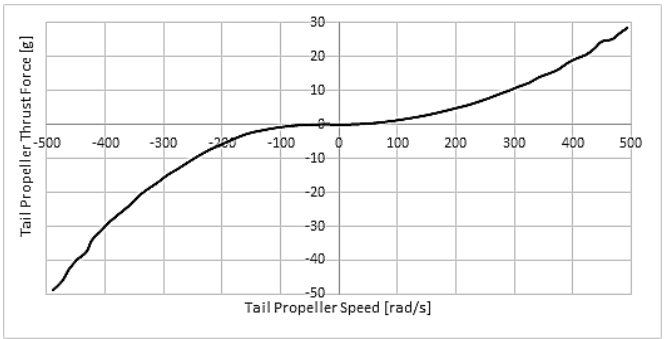

Figure 17. Tail propeller real speed/Output thrust relationship

Figure 18 shows a comparison between real data obtained from the tail propeller thrust test and, the generated model for the tail propeller thrust-speed relation. From the graph, it's shown that the model is 90% fitted with the real data.

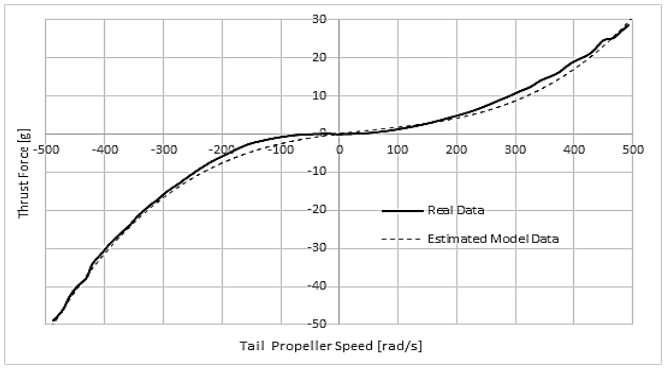

Figure 18. Tail propeller real speed/Output thrust relationship vs model

Figure 19 explains the relation between the coupling force generated on the tail propeller due to the rotation of the main propeller. The data in this graph are the real measurements excluded from the tail propeller coupling test due to main rotation. This graph is used to generate an estimated model for the coupling force generated on the tail propeller due to the rotation of the main rotor.

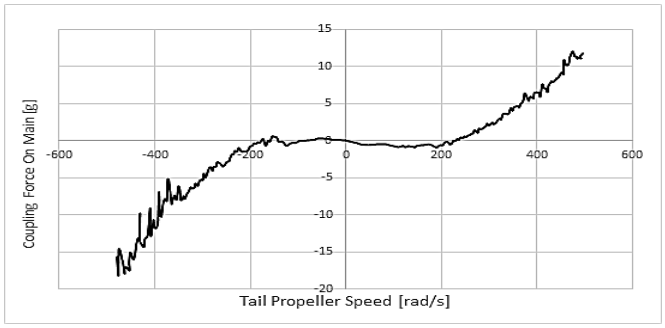

Figure 19. Real tail rotor speed/Coupling force on main relationship

Figure 20 shows a comparison between real data obtained from the coupling force on main due to tail propeller rotation and the generated model. From the graph, it's shown that the model is 89% fitted with the real data.

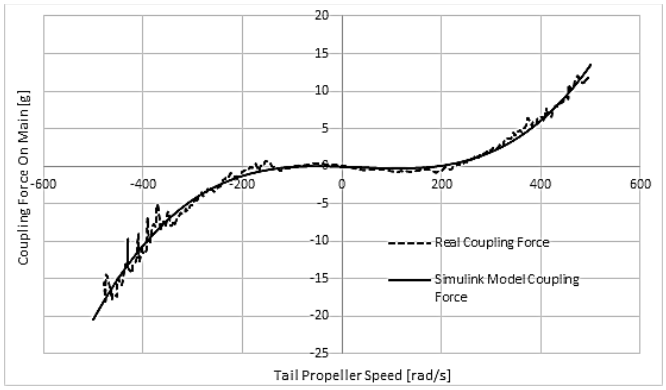

Figure 20. Real tail rotor speed/Coupling force on main relationship vs model

Figure 21 explains the relation between the coupling force generated on the main propeller due to the rotation of the tail propeller. These data in this graph are the real measurements excluded from the main propeller coupling test due to tail rotation. This graph is used to generate an estimated model for the coupling force generated on the main propeller due to the rotation of the tail rotor.

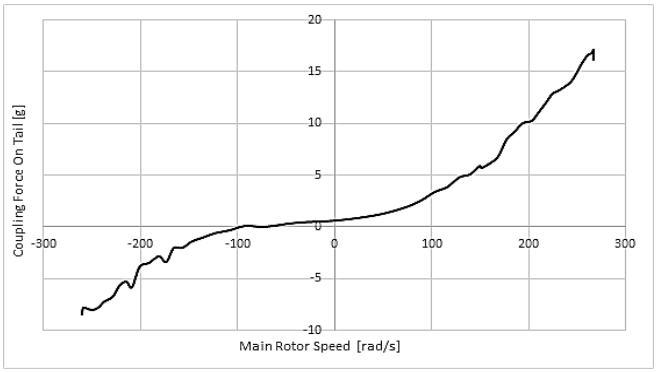

Figure 21. Tail propeller real main rotor speed/Coupling force on tail relationship

Figure 22 shows a comparison between real data obtained from the coupling force on tail due to main propeller rotation and the generated model. From the graph, it's shown that the model is 91% fitted with the real data.

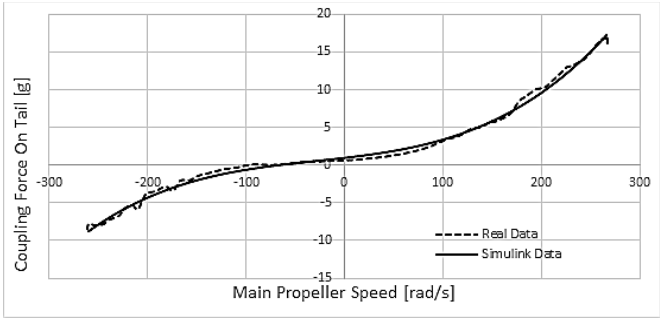

Figure 22. Tail propeller real main rotor speed/Coupling force on tail relationship vs model

Figure 23 displays the relation between the TRMS pitch angle and time due to free oscillation test. The data from this graph are used to estimate damping coefficient for the TRMS in pitch direction.

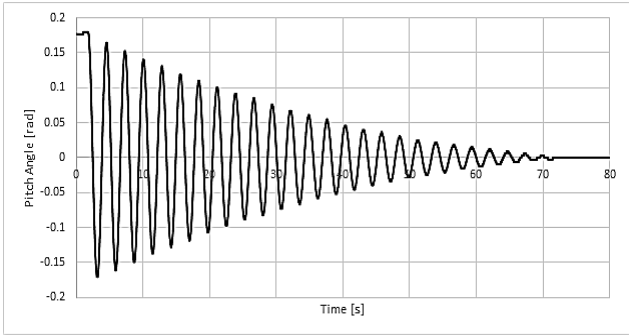

Figure 23. TRMS 10° free oscillation response in pitch direction

Figure 24 for the positive and negative peak values excluded from the TRMS 10° free oscillation response in pitch direction. These values are used for the estimation process of the damping coefficient for the TRMS in pitch direction.

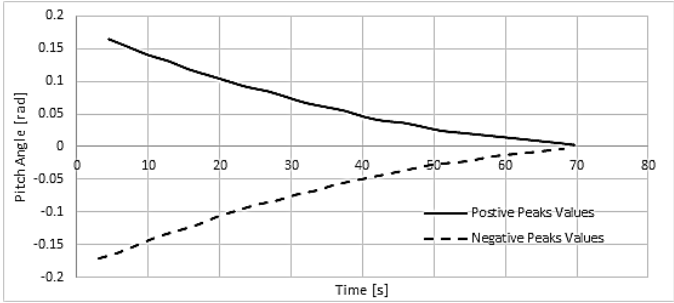

Figure 24. Negative and positive peaks values obtained from TRMS 10° free oscillation response in pitch direction

Figure 25 displays a comparison between the real measurements obtained from the TRMS 10° free oscillation response in pitch direction and a model for the TRMS 10° free oscillation based on the estimated damping coefficient in pitch direction. The graph shows that both the model data and the real data are mainly fitted in the first 10 second, where the effect of the air resistance compared with the TRMS inertia is negligible.

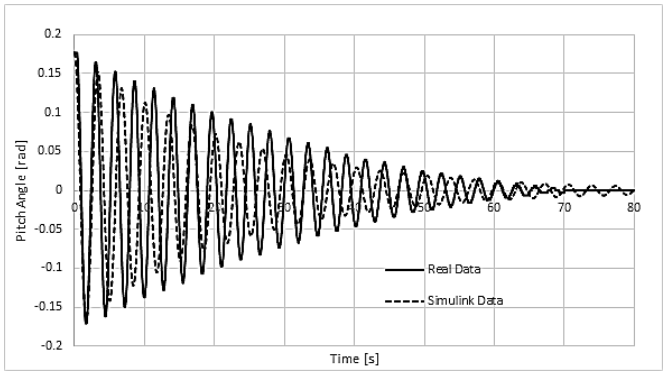

Figure 25. Real TRMS 10° free oscillation response vs model in pitch direction

Figure 26 displays the relation between the TRMS yaw angle and time due to free oscillation test. The data from this graph are used to estimate damping coefficient for the TRMS in yaw direction.

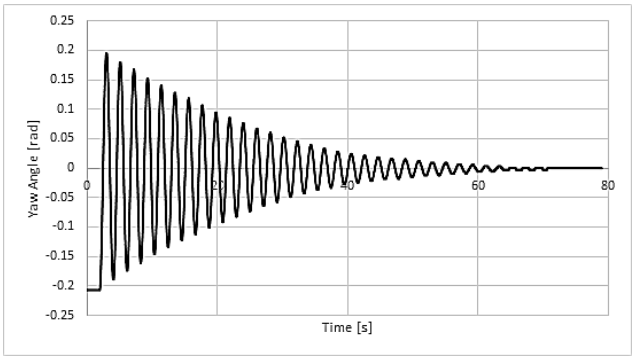

Figure 26. TRMS 10° free oscillation response in yaw direction

Figure 27 for the positive and negative peak values excluded from the TRMS 10° free oscillation response in yaw direction. These values are used for the estimation process of the damping coefficient for the TRMS in yaw direction.

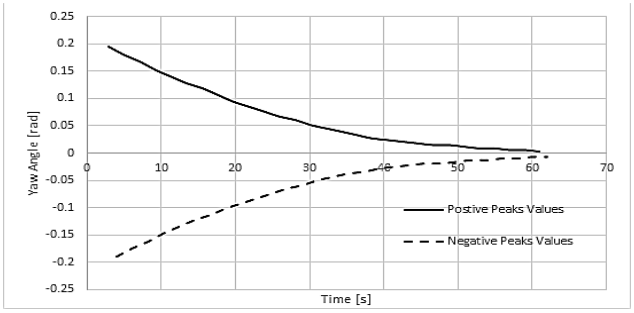

Figure 27. Negative and positive peaks values obtained from TRMS 10° free oscillation response in yaw direction

Figure 28 displays a comparison between the real measurements obtained from the TRMS 10° free oscillation response in yaw direction and a model for the TRMS 10° free oscillation based on the estimated damping coefficient in yaw direction. The graph shows that both the model data and the real data are mainly fitted in the first 10 second, where the effect of the air resistance compared with the TRMS inertia is negligible.

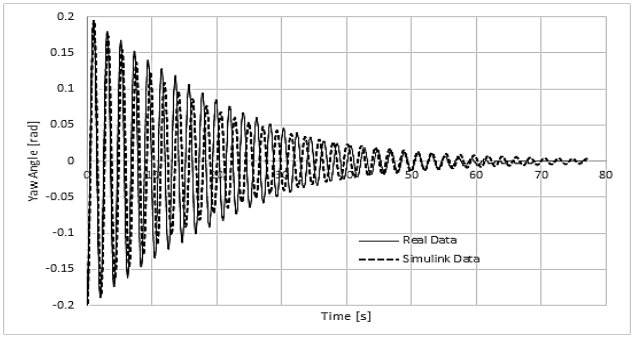

Figure 28. Real TRMS 10° free oscillation response vs model in yaw direction

VI. CONCLUSION

In this paper a mathematical model for the whole twin rotor system is built. The generated model based real data obtained from system identification process of some of the TRMS subsystems while the other relations are obtained from of physical relationship obtained from newton laws of motion. In order identify the TRMS parts, the whole TRMS is dissembled into separate subsystems, these subsystems are identifying separately based on input/output relationship. A step input signal is chosen to be the main signal for the estimation process of the mathematical model of each of the TRMS sperate parts, while a square signal is chosen to be the main signal for the validation process of each of the estimated mathematical model. A special test rig and component are added externally to help the extraction of the the input/output relationship of the TRMS separate parts. All the data obtained from the real test of the whole TRMS subsystems are exported to MATLAB system identification toolbox and MATLAB curve fitting tool box to generate an accurate and precise mathematical relation for these subsystems. The obtained models for the whole TRMS subsystem are then aggregated and linked with physical laws to build a complete and accurate model for the whole TRMS. The generated model for the TRMS is tested and simulated under MATLAB SIUMLINK environment.

REFERENCES

[1] R. W. Prouty and H. C. Curtiss Jr., "Helicopter control systems: A history," J. Guid. Control. Dyn., vol. 26, no. 1, pp. 12–18, Jan. 2003.

[2] C. C. Tsai, Z. C. Wang, C. T. Lee, and Y. Y. Li, "Intelligent adaptive trajectory tracking control for an autonomous small-scale helicopter using fuzzy basis function networks," Asian J. Control, vol. 17, no. 1, pp. 234–245, 2015.

[3] F. E. Tomlinson, "Fire fighting helicopter," Oct. 1976.

[4] T. B. Pasic and T. J. Poulton, "The Hospital-Based Helicopter: A Threat to Hearing?," Arch. Otolaryngol., vol. 111, no. 8, pp. 507–508, Aug. 1985.

[5] F. Castelluccio, L. Maritano, S. Amoroso, and M. Migliore, "Cost analysis for a future helicopter for passenger transport," Aircr. Eng. Aerosp. Technol., vol. 87, no. 2, pp. 139–146, Mar. 2015.

[6] M. Molinier, T. Hame, and H. Ahola, "3D-connected components analysis for traffic monitoring in image sequences acquired from a helicopter," Image Anal. Proc., vol. 3540, pp. 141–150, 2005.

[7] Feedback Instruments Limited, "Twin Rotor MIMO System Installation and Commissioning Manual 33-007-0M5," vol. 44, no. 1160, 1992.

[8] S. M. Ahmad, A. J. Chipper, and M. O. Tokhi, "Dynamic modelling and linear quadratic Gaussian control of a twin-rotor multi-input multi-output system," vol. 217, pp. 203–227, 2003.

[9] A. Rahideh, M. H. Shaheed, and H. J. C. Huijberts, "Dynamic modelling of a TRMS using analytical and empirical approaches," Control Eng. Pract., vol. 16, no. 3, pp. 241–259, 2008.

[10] F. M. Aldebrez, I. Z. M. Dams, and M. Tokhi, "Dynamic modelling of a twin rotor system in hovering position," pp. 823–826.

How to Cite this Article:

Kandel, M. A. O., Elsamanty, M., AbdRaboo, S. &. Hossamel-din, Y. H. (2019) A Complete Identification Methodology for Identifying Parameters of Twin Rotor Multi Input Multi Output System (TRMS). International Journal of Science and Engineering Investigations (IJSEI), 8(91), 187-196. http://www.ijsei.com/papers/ijsei-89119-25.pdf